

## Polycrystallinity Enhances Stress Buildup around Ice

Dominic Gerber<sup>1</sup>,<sup>1</sup> Lawrence A. Wilen,<sup>2</sup> Eric R. Dufresne<sup>1</sup>,<sup>1</sup> and Robert W. Style<sup>1</sup>

<sup>1</sup>*Department of Materials, ETH Zürich, 8093 Zürich, Switzerland*

<sup>2</sup>*Center for Engineering Innovation and Design, School of Engineering and Applied Sciences, Yale University, New Haven, Connecticut 06520, USA*

 (Received 23 March 2023; revised 11 August 2023; accepted 8 September 2023; published 16 November 2023)

Damage caused by freezing wet, porous materials is a widespread problem but is hard to predict or control. Here, we show that polycrystallinity significantly speeds up the stress buildup process that underpins this damage. Unfrozen water in grain-boundary grooves feeds ice growth at temperatures below the freezing temperature, leading to fast stress buildup. These stresses can build up to levels that can easily break many brittle materials. The dynamics of the process are very variable, which we ascribe to local differences in ice-grain orientation and to the surprising mobility of many grooves—which further accelerates stress buildup. Our Letter will help understand how freezing damage occurs and in developing accurate models and effective damage-mitigation strategies.

DOI: [10.1103/PhysRevLett.131.208201](https://doi.org/10.1103/PhysRevLett.131.208201)

Damage caused by ice growth can arise by two mechanisms. When water freezes in a closed system, like a full bottle of water, damage occurs due to the  $\sim 9\%$  volumetric expansion. This expansion pushes on the water's surroundings, causing the pressure to rise. While the water remains partially unfrozen, this pressure will continue to increase by  $\sim 11$  MPa per degree of undercooling [1]. This mechanism is almost unique to ice: Most liquids shrink as they freeze, reducing their pressure until the liquid cavitates [2,3]. When water instead freezes in an open system, such as in soil pores, damage can occur through the lesser-known process of *cryosuction* [4–8]. Now, water can flow away as ice grows, preventing pressure buildups during ice's initial growth. However, if the ice is below its freezing temperature and in contact with an unfrozen supply of water, it will subsequently suck water back into the pore, causing the ice to grow [6,9,10]. Then, the ice can push open the pore, causing pressure to build up with a maximum pressure of about 1 MPa per degree of undercooling [1,5,9,11–14]. Importantly, the pore expansion due to cryosuction can theoretically be unbounded, provided enough unfrozen water is available. Cryosuction is responsible for much of the damage caused by freezing wet, porous solids [8,11,12,15,16] and occurs in any liquid [17–19].

Although the basic mechanisms underlying freezing-induced stresses are well understood, it is challenging to reliably predict how and where these appear. For example, for freezing of a particular soil type, one cannot predict how fast and in what form ice will grow [15,16,20–23]. This is despite the availability of a wide range of frost-heave models (e.g., [5,6,11,14,19,21–36]). Thus, our understanding of freezing is almost exclusively empirical—in fields ranging from civil engineering and road design to cryopreservation, agriculture, food science, medicine, and

low-temperature biology [15,20,37,38]. This suggests some aspects of the freezing process are not fully understood.

Here, we show that ice polycrystallinity, a typically overlooked factor, can play a dramatic role by accelerating the buildup and expanse of freezing stresses. Water-filled grain-boundary grooves in ice act as conduits that feed ice growth across the surface of polycrystalline ice. This process can cause large, highly localized stresses which can lead to damage. The dynamics of the stress buildup can vary greatly between grooves, but the resulting stresses are always larger than stresses that appear around monocrystalline ice. Furthermore, we observe that many grooves are (often unpredictably) mobile, and these grooves support even faster ice growth, with greater damage potential.

We study the role of polycrystallinity in freezing damage by growing ice in the setup shown in Fig. 1(a) [9]. This consists of an open-ended, water-filled Hele-Shaw cell with a lower surface coated in a soft, silicone layer. The cell is placed in a temperature gradient, so that ice fills the cell's left-hand side, when viewed in the  $x, y$  plane (see Fig. 1). Any stresses that develop around the ice can be observed as deformations in the silicone. We measure these with a confocal microscope by imaging the 3D positions of fluorescent nanoparticles that are attached to the top and bottom of the silicone layer [39]. This allows us to calculate displacement maps of the silicone surface and corresponding maps showing the stress buildup around the ice. Stresses are calculated from displacements via traction force microscopy (TFM), essentially by solving an elasticity problem (see Refs. [9,40,47]). Stress and displacement maps show similar qualitative features (see Fig. S2 in Supplemental Material [40]), but stress maps have lower resolution due to smoothing in the TFM algorithm.

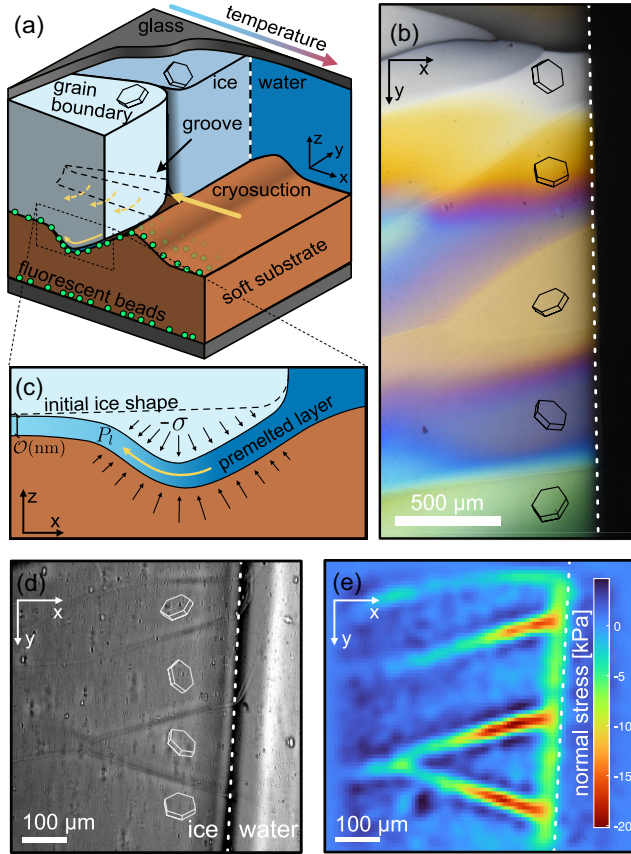


FIG. 1. (a) Schematic of polycrystalline ice in the experimental cell. (b) An ice-water interface imaged through crossed polarizers, highlighting individual grains with different crystal orientations. (c) Schematic of the cryosuction process into a premelted layer. (d) Grain boundaries (thin lines) in a bright-field micrograph of ice in the cell. (e) Stresses below the ice in (d). The image is taken 10 min after the start of the experiment. Substrate stiffness, 265 kPa; substrate thickness, 130  $\mu\text{m}$ ; ice thickness, 500  $\mu\text{m}$ ; temperature gradient, 0.4 K/mm. Crystal symbols are illustrative.

Therefore, here, we predominantly present displacement data.

Ice that forms in the cell is naturally polycrystalline. Ice grains are randomly oriented and have an average size of  $O(100 \mu\text{m})$ , comparable to the cell thickness [48]. They naturally form one layer in the cell, with their grain boundaries oriented vertically [40]. Individual grains appear with different colors in crossed polarizers [Fig. 1(b)] [9,49,50]. At the same time, water appears black—the bulk ice-water boundary is the dashed white line in Fig. 1. Grain boundaries can also be seen without polarizers, as they appear as darker lines in images [Fig. 1(d)].

We perform experiments by growing ice to the cell middle and then holding it fixed in a constant temperature gradient. When ice appears, it initially exerts only minor stresses on its surroundings (see Supplemental Fig. S3 [9]), but subsequently these stresses grow steadily. Figure 1(e) shows the normal stresses exerted by the ice on the

underlying substrate, 10 min after initial ice formation. We see a small stress buildup just on the cold side of the ice-water interface—a vertical green band. This type of “ice-front” stress buildup has been previously reported [9,10,51]. However, these stresses are dwarfed by the stresses under the grain boundaries, which are up to 5 times larger— $O(20 \text{ kPa})$ . The grain-boundary stresses also extend back to cold temperatures, causing stress buildup across a broad area of ice-substrate interface.

Stress development is caused by the localized accumulation of ice, fed by unfrozen water at the ice substrate. This water appears in two forms. First, nanometric, *premelted layers* of water exist between ice and a neighboring substrate [Fig. 1(c) [19,52,53]]. Such a layer is stabilized by a repulsive disjoining pressure between the ice and substrate. The disjoining pressure effectively reduces the hydrodynamic pressure in the premelted layer, causing water to be dragged in from nearby sources of bulk water and feeding local ice growth [6,54]. This mechanism underlies the ice-front stress band in Fig. 1(e). These premelted films thicken into macroscopic “grain-boundary grooves” at the triple junction where two ice grains meet at a substrate [Fig. 1(a)]. These grooves, the second form of unfrozen water below  $0^\circ\text{C}$ , occur due to the ice-water interface’s surface energy [55–57], analogously to plateau borders in foams. In our experiments, grooves are always much larger than premelted films: 100 nm radius tracer particles are easily transported along them (Supplemental Video 1 [40]). This matches our expectations, as groove width should decrease inverse proportionally to undercooling [56] and be  $\gtrsim 1 \mu\text{m}$  in our field of view [40].

Stress development at grain-boundary grooves appears to be driven by ice growth at their sides. This is clear when we observe “giant,” faceted grooves. In these rare grooves, adjoining ice grains expose their basal facet toward the groove [40]. The basal facets grow only at a larger undercooling of  $\sim 0.03^\circ\text{C}$ , yielding grooves that are much larger than ordinary grooves [56,58,59]. Figure 2 shows examples of ordinary and giant grooves, along with the associated substrate indentations. The indentation under the ordinary groove appears as a single trough. However, under the giant groove, the ice grows only into the substrate at the groove edges. In the middle of the giant groove, the substrate actually bulges back upward—as shown in Fig. 2(f), with a schematic cross section through a groove (green dots show experimental data). This indicates that stresses build up only at the groove sides, where ice and substrate come into close contact. Here, there is a premelted layer, which can drag in water to feed ice growth via the same mechanism underlying ice-front stress buildup [compare Fig. 1(c) with Figs. 2(e) and 2(f)]. We expect that something similar occurs at ordinary grooves [Fig. 2(e)] but that the scale is too small to resolve individual bulge and troughs.

Indentations under the ice continuously grow, while the extent of the indented area gradually expands (Supplemental

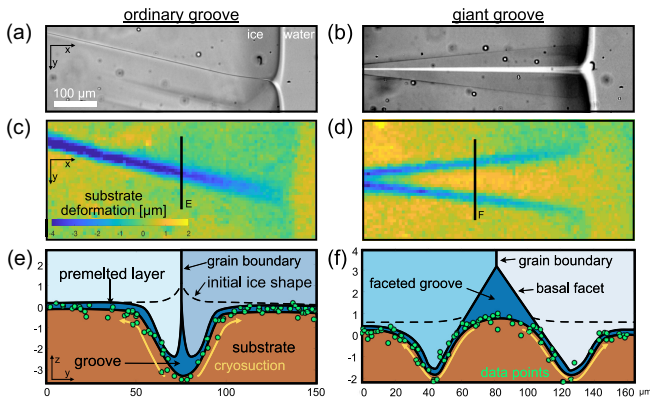


FIG. 2. (a),(b) Bright-field images of ordinary and giant grooves. (c),(d) Substrate indentations caused by ice growth. (e),(f) Cross sections through the data at the lines indicated in (c), (d), with corresponding groove schematics. Giant grooves have basal facets as their walls, while ordinary grooves are unafaceted. Images are 30 min after the experiment starts. Substrate stiffness, 38 kPa; substrate thickness, 100  $\mu\text{m}$ ; ice thickness, 200  $\mu\text{m}$ ; temperature gradient, 0.1 K/mm. Substrate stiffness was chosen so as to easily visualize stresses [9].

Video 2 [40]). For example, Fig. 3(a) shows evolving surface indentations under the center of a stationary grain boundary. For comparison, the much smaller indentations that form away from the grain boundaries are shown at the last time point (dotted curves,  $t = 360$  min). All curves exhibit a maximum indentation away from the bulk ice-water interface ( $x = 0$ ), and this continuously grows, while the indentation spreads to colder temperatures. Close to the ice-water interface (within  $\sim 50$   $\mu\text{m}$ ), ice growth appears to stall, consistent with the expectation of a temperature-dependent stall stress that is predicted to increase linearly with undercooling [1,9].

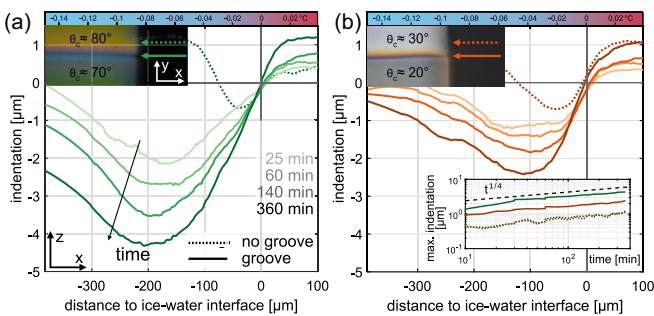


FIG. 3. Evolution of indentations under (continuous curves) and parallel to (dashed curves) two grain-boundary grooves [(a) and (b), respectively] under identical experimental conditions. Insets, top left: two images through crossed polarizers, showing the grain boundaries.  $\theta_c$  is the angle between the ice-crystal  $c$  axis and the substrate, estimated from the birefringence color [9]. Inset in (b): evolution of the maximum indentation. The dashed line shows a power law as a guide to the eye. Substrate stiffness, 280 kPa; substrate thickness, 100  $\mu\text{m}$ ; ice thickness, 500  $\mu\text{m}$ ; temperature gradient, 0.4 K/mm.

While the qualitative features of ice growth are repeatable, the dynamics can vary greatly between grooves. Figure 3(b) shows a stationary groove near the one in Fig. 3(a) but between crystals of different orientations. The indentation below this groove is much smaller, suggesting that grain orientation may play an important role in the dynamics of stress buildup. The inset in Fig. 3 shows the maximum indentation under the two grooves (continuous curves). Interestingly, both exhibit approximately power-law indentation growth, with exponents  $\sim 0.25$ , while the indentations far from grooves also follow this power law (dashed curves). This might be expected, as theory often predicts power-law behavior in similar processes [34]. However, the power-law exponent is not fixed and varies in further experiments between 0.25 and 0.33 (see Supplemental Fig. S4 [40]).

Most grain boundaries at the ice-water interface are also mobile, and this can significantly accelerate stress accumulation (see Supplemental Material [40] for statistics regarding grain-boundary mobility). We observe that grain boundaries can translate steadily, move with stop-start motion, oscillate about a fixed position, oscillate intermittently, exhibit unpredictable combinations of the above, or fuse with other grain boundaries [e.g., Figs. 4(a)–4(c) and

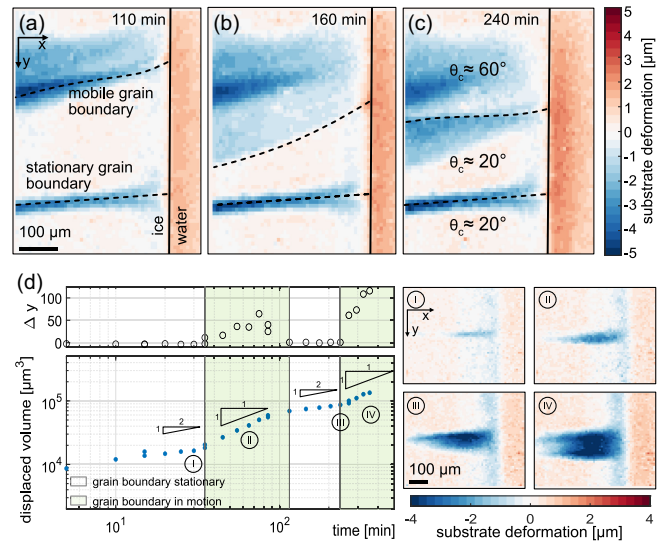


FIG. 4. (a)–(c) Substrate indentations below ice with a stationary (bottom) and a mobile (top) grain boundary moving in a stop-start fashion (Supplemental Video 2 [40]). Dashed curves show the current grain boundary locations. Ice thickness,  $\sim 200$   $\mu\text{m}$ ; substrate stiffness, 52 kPa; substrate thickness, 45  $\mu\text{m}$ ; temperature gradient, 0.1 K/mm. (d) Change in displaced volume below a sporadically moving groove (green sections indicate motion). Approximate local power laws are given as guides to the eye. Top panel: the  $y$  position of the grain boundary close to the bulk ice-water interface. Panels I–IV show surface displacements at the corresponding time points. Ice thickness,  $\sim 500$   $\mu\text{m}$ ; substrate stiffness, 52 kPa; substrate thickness, 45  $\mu\text{m}$ ; temperature gradient, 0.1 K/mm.

Supplemental Videos 2–5 [40]). This is important, as ice growth rates are enhanced under mobile grain boundaries. For example, Fig. 4(d) shows the total accumulated ice volume  $V$  under a sporadically moving grain boundary.  $V$  increases significantly faster in mobile phases than in stationary phases. Ice growth always occurs directly at grain boundaries and does not melt back if the grain boundary moves on. Thus, mobile grain boundaries result in widely distributed stresses [e.g., Figs. 4(a)–4(c) and Supplemental Videos 2 and 3 [40)] and have a very different damage potential than stationary grooves.

Grain-boundary motion appears to be controlled by grain orientation and the presence of a soft substrate. We always observe initial motion driven by grain coarsening [48,60–66], whether in silicone-coated cells or in glass-walled cells (e.g., Supplemental Video 5 [40]). Subsequently, ice in glass cells shows no movement, while ice in silicone cells exhibits the unpredictable motion described above [40]. This suggests the presence of substrate-mediated grain-boundary instabilities—indeed, sudden jumps in grain-boundary position were often accompanied by abrupt changes in substrate deformations (Supplemental Fig. 6 [40]). In general, boundaries between grains with large differences in crystallographic orientation were more mobile than boundaries between grains with similar orientations (e.g., Fig. 4), in agreement with previous theoretical predictions [66].

We can qualitatively explain many of our observations using existing cryosuction theory [1,5,6,27,29,36]. This suggests that ice will continue to grow by suction into films, until it reaches a temperature-dependent stress given by the Clapeyron equation describing thermodynamic equilibrium between ice and water:

$$-\sigma - P_a = \rho q_m \frac{T_m - T}{T_m}. \quad (1)$$

Here,  $\rho$  and  $q_m$  are the density and latent heat of melting of ice, respectively,  $T_m$  is the bulk freezing temperature at atmospheric pressure,  $P_a$  is the pressure of the nearby bulk-water source (here, atmospheric pressure), and  $\sigma$  is the normal stress exerted by the ice on the substrate ( $\sigma < 0$  when compressing the substrate) [1,9]. Inserting typical values, we find that the extra pressure exerted by ice on the substrate ( $-\sigma - P_a$ ) can be up to 1 MPa per degree of undercooling. Hence, we observe larger stresses at the undercooled grain boundaries than we observe near the warmer bulk ice-water interface [e.g., Fig. 1(e)].

Although the Clapeyron equation tells us the maximum stress that can occur in freezing systems, ultimately stress buildup is governed by water transport. Water cannot travel large distances along nanoscopic, premelted films due to viscous drag [5,6,10,34]: Flow rates scale  $\sim h^3$ , where  $h$  is film thickness, and, thus, flow drops off dramatically as the films thin [55]. Thus, we see ice buildup only very close to

the bulk ice-water interface in the absence of nearby grooves, and ice buildup slows at colder temperatures, where premelted films are thinner [52]. Additionally, the flow rate dependence on film thickness means that we expect large differences in how stress builds up at differently oriented grains. This is because premelted film thicknesses at a substrate are known to depend strongly on local ice-grain orientation [52,67,68]. Indeed, this orientation dependence could explain the variability we see in our experiments. In future, carefully observing the effects of grain orientation may offer a way to measure a premelted film’s thickness dependence on temperature and grain orientation—an important, but poorly characterized, property for topics ranging from ice rheology to cryobiology and food science [51,52,69,70].

Most importantly, the novel function of grooves is to transport bulk water to colder temperatures, where large stresses can build up directly adjacent to the grooves. This buildup should continue to occur, provided that premelted film thicknesses do not vanish. Although the critical temperature where this occurs is not precisely known, it is almost always measured as being below  $-5^\circ\text{C}$  [52,71–73]. Thus, ice should be able to accumulate near grooves down to at least  $-5^\circ\text{C}$ , with associated stresses reaching up to 5 MPa. This can easily break many stiff, brittle materials and makes the mechanism we describe here particularly dangerous.

In conclusion, freezing-induced stress buildup is dramatically accelerated in polycrystalline ice relative to monocrystalline ice. Grain-boundary grooves act as conduits for unfrozen water that feed ice growth across ice-substrate interfaces. This growth is very localized to the grooves and can quickly reach pressures of several tens of kPa—here, within minutes. Ultimately, this mechanism can feed stress buildup up to the limit given by the Clapeyron equation. Thus, in typical freezing conditions, stresses can reach several MPa, and this mechanism is capable of breaking many materials. The rapid stress buildup around grooves (the dynamics of which should depend on the local temperature gradient [9]) means that this process can play a key role in stress development and should be accounted for in models. Interestingly, we see large variability in how fast stress builds up, and this may explain difficulties in producing accurate freezing models. Thus, a key question is whether there is a predictable average behavior to allow incorporation into models. We ascribe stochasticity in stress buildup to differences in ice-grain orientation and to the mobility of some grain boundaries (which is strongly amplified by the presence of a soft substrate). Understanding these factors should give rich insights into the freezing process.

Our results have important consequences for understanding freezing damage. The pressure distribution applied by ice to a confining material will determine how this material breaks. Thus, especially in brittle materials, stress localization at grooves may play a key

role in determining when and how damage occurs. Additionally, we expect ice's growth history to affect stress buildup. Fine-grained ice will have more grooves where stress can develop than coarser-grained ice and, thus, should exert more cumulative forces on its surroundings. Ice nucleated at large undercoolings will tend to form many small grains, while slowly grown ice will have fewer, large grains. Thus, altering how ice forms and ages could alter how stress builds up. The stress buildup process should significantly change in the presence of chemicals that bind to different ice facets and inhibit recrystallization (e.g., antifreeze proteins [74–77]). Finally, we anticipate that this ice-growth process will also occur by water-filled veins between grains in the ice bulk and by small, unfrozen pores in frozen porous materials. Cryosuction into premelted films adjacent to these supplies of bulk water would increase ice-growth rates, driving even faster stress accumulation.

We thank Christine McCarthy and Charlotta Lorenz for helpful discussions. We acknowledge support from an ETH Research Grant (ETH-38 18-2) and the Swiss National Science Foundation (200021-212066).

- 
- [1] R. W. Style, D. Gerber, A. W. Rempel, and E. R. Dufresne, *J. Glaciol.* **69**, 1901 (2023).
- [2] F. Kohler, L. Gagliardi, O. Pierre-Louis, and D. Dysthe, *Phys. Rev. Lett.* **121**, 096101 (2018).
- [3] M. Scoti, F. De Stefano, A. Giordano, G. Talarico, and C. De Rosa, *Polymers* **14**, 4032 (2022).
- [4] F. Unold and L. Derk, in *PanAm Unsaturated Soils 2017* (American Society of Civil Engineers, Dallas, TX, 2018), pp. 290–299, [10.1061/9780784481691.029](https://doi.org/10.1061/9780784481691.029).
- [5] B. Derjaguin and N. Churaev, *Cold Reg. Sci. Technol.* **12**, 57 (1986).
- [6] J. Wettlaufer and M. G. Worster, *Annu. Rev. Fluid Mech.* **38**, 427 (2006).
- [7] H. Ozawa and S. Kinoshita, *J. Colloid Interface Sci.* **132**, 113 (1989).
- [8] O. Coussy, *Mechanics and Physics of Porous Solids: Coussy/Mechanics and Physics of Porous Solids* (John Wiley & Sons, Ltd, Chichester, UK, 2010).
- [9] D. Gerber, L. A. Wilen, F. Poydenot, E. R. Dufresne, and R. W. Style, *Proc. Natl. Acad. Sci. U.S.A.* **119**, e2200748119 (2022).
- [10] L. A. Wilen and J. G. Dash, *Phys. Rev. Lett.* **74**, 5076 (1995).
- [11] P. Wang and G. Zhou, *Int. J. Min. Sci. Technol.* **28**, 287 (2018).
- [12] J. S. Wettlaufer, J. G. Dash, and N. Untersteiner, *Ice Physics and the Natural Environment* (Springer Science & Business Media, New York, 2013).
- [13] P. B. Black, Applications of the Clapeyron Equation to Water and Ice in Porous Media, Technical Report No. 95-6, Cold Regions Research and Engineering Laboratory, 1995.
- [14] S. Kjelstrup, S. A. Ghoreishian Amiri, B. Loranger, H. Gao, and G. Grimstad, *Acta Geotech.* **16**, 2231 (2021).
- [15] M. Carter and S. P. Bentley, *Soil Properties and Their Correlations*, 1st ed. (Wiley, New York, 2016), [10.1002/9781119130888](https://doi.org/10.1002/9781119130888).
- [16] J. G. Dash, A. W. Rempel, and J. S. Wettlaufer, *Rev. Mod. Phys.* **78**, 695 (2006).
- [17] S. Taber, *J. Geol.* **38**, 303 (1930).
- [18] M. Hiroi, T. Mizusaki, T. Tsuneto, A. Hirai, and K. Eguchi, *Phys. Rev. B* **40**, 6581 (1989).
- [19] J. G. Dash, in *Phase Transitions in Surface Films 2*, NATO ASI Series, edited by H. Taub, G. Torzo, H. J. Lauter, and S. C. Fain (Springer, Boston, 1991), pp. 339–356.
- [20] A. F. DiMillio, A quarter century of geotechnical research, Technical Report No. FHWA-RD-98-139, Federal Highway Administration, 1999, <https://www.fhwa.dot.gov/publications/research/infrastructure/geotechnical/98139/01.cfm>.
- [21] S. S. L. Peppin and R. W. Style, *Vadose Zone J.* **12**, 1 (2013).
- [22] R. W. Style and S. S. L. Peppin, *J. Fluid Mech.* **692**, 482 (2012).
- [23] K. O'Neill, *Cold Reg. Sci. Technol.* **6**, 275 (1983).
- [24] J. M. H. Schollick, R. W. Style, A. Curran, J. S. Wettlaufer, E. R. Dufresne, P. B. Warren, K. P. Velikov, R. P. A. Dullens, and D. G. A. L. Aarts, *J. Phys. Chem. B* **120**, 3941 (2016).
- [25] J. You, J. Wang, L. Wang, Z. Wang, J. Li, and X. Lin, *Colloids Surf. A* **553**, 681 (2018).
- [26] K. Watanabe and M. Mizoguchi, *Cold Reg. Sci. Technol.* **34**, 103 (2002).
- [27] J. Zhou and C. Wei, *Cold Reg. Sci. Technol.* **171**, 102964 (2020).
- [28] M. Vignes and K. M. Dijkema, *J. Colloid Interface Sci.* **49**, 165 (1974).
- [29] R. R. Gilpin, *Water Resour. Res.* **16**, 918 (1980).
- [30] A. W. Rempel, *Quat. Res.* **75**, 316 (2011).
- [31] J.-M. Konrad and N. R. Morgenstern, *Can. Geotech. J.* **17**, 473 (1980).
- [32] J. S. Wettlaufer, M. G. Worster, L. A. Wilen, and J. G. Dash, *Phys. Rev. Lett.* **76**, 3602 (1996).
- [33] I. Vlahou and M. G. Worster, *Proc. R. Soc. A* **471**, 20140741 (2015).
- [34] J. S. Wettlaufer and M. G. Worster, *Phys. Rev. E* **51**, 4679 (1995).
- [35] L. Gagliardi and O. Pierre-Louis, *Europhys. Lett.* **127**, 59002 (2019).
- [36] D. H. Everett, *Trans. Faraday Soc.* **57**, 1541 (1961).
- [37] E. E. Benson, in *Plant Cryopreservation: A Practical Guide*, edited by B. M. Reed (Springer, New York, 2008), pp. 15–32, [10.1007/978-0-387-72276-4\\_2](https://doi.org/10.1007/978-0-387-72276-4_2).
- [38] S. Deville, *Freezing Colloids: Observations, Principles, Control, and Use: Applications in Materials Science, Life Science, Earth Science, Food Science, and Engineering*, Engineering Materials and Processes (Springer International Publishing, Cham, 2017), [10.1007/978-3-319-50515-2](https://doi.org/10.1007/978-3-319-50515-2).
- [39] Y. Xu, W. C. Engl, E. R. Jerison, K. J. Wallenstein, C. Hyland, L. A. Wilen, and E. R. Dufresne, *Proc. Natl. Acad. Sci. U.S.A.* **107**, 14964 (2010).
- [40] See Supplemental Material at <http://link.aps.org/supplemental/10.1103/PhysRevLett.131.208201> for a brief description, which includes Refs. [41–46].
- [41] R. W. Style, T. Sai, N. Fanelli, M. Ijavi, K. Smith-Mannschott, Q. Xu, L. A. Wilen, and E. R. Dufresne, *Phys. Rev. X* **8**, 011028 (2018).

- [42] J. D. Harrison and W. A. Tiller, *J. Appl. Phys.* **34**, 3349 (1963).
- [43] P. D. Garcia and R. Garcia, *Biophys. J.* **114**, 2923 (2018).
- [44] S. Hell, G. Reiner, C. Cremer, and E. H. K. Stelzer, *J. Microsc.* **169**, 391 (1993).
- [45] T. Besseling, J. Jose, and A. van Blaaderen, *J. Microsc.* **257**, 142 (2015).
- [46] B. Sabass, M. L. Gardel, C. M. Waterman, and U. S. Schwarz, *Biophys. J.* **94**, 207 (2008).
- [47] R. W. Style, R. Boltyskiy, G. K. German, C. Hyland, C. W. MacMinn, A. F. Mertz, L. A. Wilen, Y. Xu, and E. R. Dufresne, *Soft Matter* **10**, 4047 (2014).
- [48] W. Mullins, *Acta Metall.* **6**, 414 (1958).
- [49] T. Zhang, L. Wang, Z. Wang, J. Li, and J. Wang, *J. Phys. Chem. B* **125**, 970 (2021).
- [50] B. E. Sørensen, *Eur. J. Mineral.* **25**, 5 (2013).
- [51] J. G. Dash, H. Fu, and J. S. Wettlaufer, *Rep. Prog. Phys.* **58**, 115 (1995).
- [52] B. Slater and A. Michaelides, *Nat. Rev. Chem.* **3**, 172 (2019).
- [53] N. V. Churaev, S. A. Bardasov, and V. D. Sobolev, *Langmuir* **10**, 4203 (1994).
- [54] L. A. Wilen, J. S. Wettlaufer, M. Elbaum, and M. Schick, *Phys. Rev. B* **52**, 12426 (1995).
- [55] R. W. Style and M. Grae Worster, *Phys. Rev. Lett.* **95**, 176102 (2005).
- [56] L. A. Wilen and J. G. Dash, *Science* **270**, 1184 (1995).
- [57] W. W. Mullins, *J. Appl. Phys.* **28**, 333 (1957).
- [58] J. G. Dash, V. A. Hodgkin, and J. S. Wettlaufer, *J. Stat. Phys.* **95**, 1311 (1999).
- [59] K. G. Libbrecht, *Annu. Rev. Mater. Res.* **47**, 271 (2017).
- [60] T. Hondoh and A. Higashi, *Philos. Mag. A* **39**, 137 (1979).
- [61] C. A. Knight, *J. Appl. Phys.* **37**, 568 (1966).
- [62] O. B. Nasello, C. L. Di Prinzio, and P. G. Guzmán, *Acta Mater.* **53**, 4863 (2005).
- [63] A. Higashi, *J. Glaciol.* **21**, 589 (1978/ed).
- [64] M. Verma, S. Sugathan, S. Bhattacharya, and R. Mukherjee, *Scr. Mater.* **209**, 114383 (2022).
- [65] K. Chen, J. Han, X. Pan, and D. J. Srolovitz, *Proc. Natl. Acad. Sci. U.S.A.* **117**, 4533 (2020).
- [66] D. Min and H. Wong, *J. Appl. Phys.* **100**, 053523 (2006).
- [67] H. Dosch, A. Lied, and J. Bilgram, *Surface Sci.* **327**, 145 (1995).
- [68] Y. Furukawa, M. Yamamoto, and T. Kuroda, *J. Cryst. Growth* **82**, 665 (1987).
- [69] B. N. J. Persson, *J. Chem. Phys.* **143**, 224701 (2015).
- [70] D. T. F. Möhlmann, *Cryobiology* **58**, 256 (2009).
- [71] V. Sadtchenko and G. E. Ewing, *Can. J. Phys.* **81**, 333 (2003).
- [72] S. Engemann, H. Reichert, H. Dosch, J. Bilgram, V. Honkimäki, and A. Snigirev, *Phys. Rev. Lett.* **92**, 205701 (2004).
- [73] H. Li, J. Mars, W. Lohstroh, M. M. Koza, H.-J. Butt, and M. Mezger, *Angew. Chem., Int. Ed.* **60**, 7697 (2021).
- [74] R. P. Tas, V. Sampaio-Pinto, T. Wennekes, L. W. van Laake, and I. K. Voets, *EMBO Rep.* **22**, e52162 (2021).
- [75] M. Bayer-Giraldi, G. Sazaki, K. Nagashima, S. Kipfstuhl, D. A. Vorontsov, and Y. Furukawa, *Proc. Natl. Acad. Sci. U.S.A.* **115**, 7479 (2018).
- [76] M. Bar Dolev, I. Braslavsky, and P. L. Davies, *Annu. Rev. Biochem.* **85**, 515 (2016).
- [77] C. A. Knight and A. Wierzbicki, *Cryst. Growth Des.* **1**, 439 (2001).